

Accepted Manuscript

Penetration behavior of reactive liner shaped charge jet impacting thick steel plates

Huanguo Guo , Yuanfeng Zheng , Qingbo Yu , Chao Ge ,
Haifu Wang

PII: S0734-743X(18)30945-X
DOI: <https://doi.org/10.1016/j.ijimpeng.2018.12.005>
Reference: IE 3215



To appear in: *International Journal of Impact Engineering*

Received date: 21 September 2018
Revised date: 6 December 2018
Accepted date: 10 December 2018

Please cite this article as: Huanguo Guo , Yuanfeng Zheng , Qingbo Yu , Chao Ge , Haifu Wang , Penetration behavior of reactive liner shaped charge jet impacting thick steel plates, *International Journal of Impact Engineering* (2018), doi: <https://doi.org/10.1016/j.ijimpeng.2018.12.005>

This is a PDF file of an unedited manuscript that has been accepted for publication. As a service to our customers we are providing this early version of the manuscript. The manuscript will undergo copyediting, typesetting, and review of the resulting proof before it is published in its final form. Please note that during the production process errors may be discovered which could affect the content, and all legal disclaimers that apply to the journal pertain.

Highlights:

- Reactive jet penetrating thick steel plates show unusual damage behaviors.
- Damage effects of thick steel plates strongly depended on reactive jet standoff.
- Model predictions of damage to thick steel plates fit well with experiments.
- Initiation delay time of reactive jet is the primary determinant mechanism.

ACCEPTED MANUSCRIPT

Penetration behavior of reactive liner shaped charge jet impacting thick steel plates

Huanguo Guo, Yuanfeng Zheng, Qingbo Yu, Chao Ge, Haifu Wang*

State Key Laboratory of Explosion Science and Technology, Beijing Institute of Technology, Beijing 100081, China

Abstract: Reactive liner shaped charge jet (RLSCJ) penetrates thick steel plate by experiments and model analysis combined. The experimental reactive material liners with a density of about 2.3 g/cm^3 , composed of mass matched ratios of Al/PTFE powders, are consolidated by a cold pressing/sintering process. Four standoffs of 0.5, 1.0, 1.5, and 2.0 CD (charge diameter) are selected to conduct the penetration experiments. The experimental results show that, compared with traditional metal liner shaped charge jet against thick steel plates, a relative larger hole diameter but lower depth accompanying with fragmentation effects of penetrating steel plates are produced by RLSCJ. To understand this penetration behavior of reactive jet, an analytical model is developed to discuss the influence of initiation delay time of reactive jet and standoff on penetration depth. Analysis shows that the penetration depth strongly depends on initiation delay time of reactive jet. With increasing the initiation delay time, the penetration depth increases significantly, showing a good agreement with the experiments. Moreover, to further understand the fragmentation mechanism effect of the thick steel plates, the effective mass of reactive jet inside the penetrating hole and its deflagration-induced structural damage effect are analyzed theoretically. Prediction results fit well with the experiments, including crack generation and propagation in the thick steel plates, and the number of fragments.

Keywords: Shaped charge, Reactive material liner, Penetration mechanics, Damage effect, Thick steel plate

1 Introduction

Traditional metal liner shaped charge jet, typically such as copper jet damages the target by producing deep penetration. However, for enhanced structural damage or fragmentation behavior, much greater effectiveness could be achieved from reactive liner shaped charge jet (RLSCJ) by releasing chemical energy within the target during or at the termination of the penetration process [1,2]. The RLSCJ produces dramatically catastrophic structural damage to concrete, masonry or geologic material targets, or greater behind-armor effects [3,4].

Over the past twenty years, high strength reactive materials and their applications have been studied extensively due to the unique performances. In general, the reactive materials are fabricated by introducing active metal powders into a polymer binder via a pressing/sintering process, typically such as Al/PTFE reactive materials [5-8]. Studies involving the mechanical properties [9-11], microstructural performance [12, 13], impact initiation [14-16], and energy release characteristics [17,18], as well as the enhanced damage effects of the targets by reactive fragments [1,19] are widely conducted, by means of drop-weight test, ballistic impact, and Taylor anvil experiments and so on. In addition, our research group has also devoted large amount of effort to investigating the properties and applications of reactive materials since the year of 2000. As a part of the effort, representative researches on reactive material

projectiles include energy release characteristics [20], behind-plate overpressure effect [21], enhanced initiation effect impacting covered explosive [22], penetration performance and enhanced damage effects of reactive material projectiles impacting single or double-spaced aluminum plates [23, 24].

Shaped charge with reactive material liners is a novel application of reactive materials, by which traditional inert metal liners were replaced to achieve greater devastating effects against many targets [25-30]. By means of the Split Hopkinson bar and quasi-static compression experiments [25], the Johnson-Cook strength model of Al/PTFE was developed to study the formation behavior of reactive jet, which fitted well with the of X-ray tests [26]. The jet characteristics of reactive material liner and mass matched aluminum liner were also presented with flash X-rays, by which the difference between tip velocity of reactive jet and aluminum jet was only 100m/s, while reactive jet produced more significant cratering and severe damage to the concrete target than aluminum jet [3]. Further research on pure concrete targets showed that the reactive liner produced a funnel shaped hole and significant demolition effect whereas the copper liner just produced a slender penetration hole and less damage [27]. Due to the excellent damaging capability, the standoff effect of reactive jet against standard concrete targets were investigated by experiments, and the results indicated that concrete damaging capability was better in a region between a half and one charge diameter of standoff [28]. The reactive material chemical reaction was not occurring significantly during jet formation, however, during or at

the termination of penetration process, both the released chemical energy and lots of gaseous product would produce catastrophic damage to the concrete targets. Under the incorporated defeat mechanisms of kinetic energy and chemical energy, the damage modes, such as demolition cavity, deflections, and cracks, of concrete targets were produced. To analyze the complicated fracture patterns of concrete targets under detonation, T. Rabczuk [31-35] proposed a dual-horizon peridynamics formulation or cracking-particle method which have been applied for a range of problems including crack propagation and crack branching. Metal targets (for example steel targets or aluminum targets) have been widely used as light armor materials, hence, it is significant and valuable to study the damage effects of reactive jet against the kind of typical targets. Different from the concrete targets, fragmentation effects of the steel targets produced by reactive jet, resulting in the penetration and defeat mechanisms are not well understood, especially the fragmentation damage capabilities have not been well characterized.

This paper presents such a research, beginning with a series of RLSCJ penetrating thick steel plates experiments. Subsequently, the influences of the initiation delay time of reactive jet and standoff on penetration depth are discussed by an analytical model developed. Finally, the fragmentation behavior of the penetrating steel plate caused by reactive jet deflagration inside the penetration hole is analyzed.

2 Experiments

2.1 Reactive material liner specimens

The processing method of the reactive material liner would consist of four steps. Firstly, the reactive liner materials were the mixture of 73.5 wt% PTFE and 26.5 wt% Al powders by mass matched ratios. The average sizes of the PTFE and Al particles were approximate 100 and 44 μm , respectively. Secondly, putting a certain amount of the mixture powers into the pre-prepared mold, and then cold isostatic pressing the powers with a corresponding top mold at a large quantity of pressures. Again, sintering the pressed reactive liner samples at a temperature of 380°C in a vacuum oven [12]. Lastly, the sintered reactive liners were re-shaped to prevent the deformation of the liner during the sintering process from affecting the formation of the jet. The density of the reactive liner was about by 2.3 g/cm^3 . The prepared reactive liners are shown in Fig.1. The experimental reactive liners were of the same shape and mass, with the base diameter of 90 mm and the wall thickness of 9 mm. The liners were precisely fabricated from performs that were well consistently characterized.



Fig.1. Reactive material liner specimens

2.2 Experimental setup

Fig.2 presents the experimental setup. Major components of shaped charge are a reactive material liner, high-energy explosive, case, and a central detonator. The height of main charge was 180 mm and the explosive was initiated by a detonator which placed on the center of the bullet. The high-energy explosive was cast into 45#

steel case with the thickness of 5 mm. In order to study the influence of RLSCJ on penetration and deflagration combined enhanced damage effects under different standoffs, aluminum standoff tubes of four different heights (0.5, 1.0, 1.5, and 2.0 CD) were used to adjust the heights from the bottom of the charge to the steel plates. The target plate was 45# steel cylinder with a 200 mm diameter and a 200 mm height.

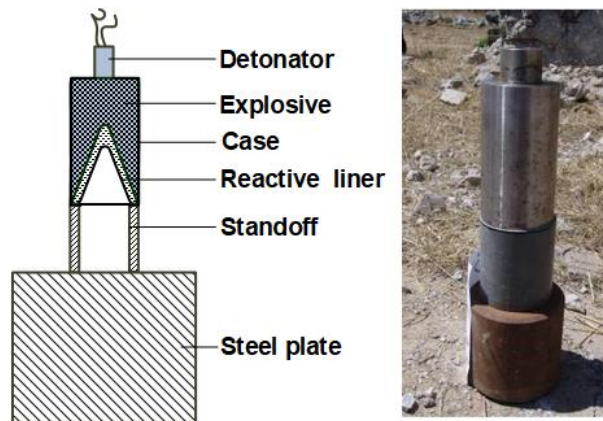


Fig.2 Experimental setup for RLSCJ penetrating thick steel plate

2.3 Experimental results

The experimental results are presented in Table 1. The results show that as the standoff increases, the penetration depth increases firstly and then decreases, and the entrance hole diameter gradually decrease. Especially, when the standoff is larger than 1.5 CD, the penetration depth decrease rapidly. The Table 1 also demonstrates that the entrance hole diameter is for greater than that caused by copper jet while the penetration depth is lower. When the standoff is 0.5 CD, the RLSCJ causes the dramatic damage effect, resulting in a maximum hole diameter of 68.6 mm at the upper surface of steel plate. Moreover, the RLSCJ penetrates the thick steel plate with the largest penetration depth of 110 mm at standoff 1.5 CD.

Table 1 Experimental results

No.	Standoff (CD)	Penetration depth (CD)	Entrance hole diameter (CD)	Fragment/ large crack numbers
1	0.5	0.93	0.76	6 fragments / 6 cracks
2	1	1.18	0.72	2 fragments / 5 cracks
3	1.5	1.22	0.67	2 fragments
4	2	0.95	0.58	2 cracks

Different damage patterns of thick steel plates are investigated by analyzing the experimental results, as shown in Fig.3. The results show that the damage to the thick steel plate is significantly influenced by reactive jet standoff. When RLSCJ penetrates thick steel plates at 0.5, 1.0, and 1.5 CD standoff, the fragmentation damage patterns are formed on the thick steel plates. Under the combined effect of kinetic and chemical energy, the steel plates are broken into several fragments. Moreover, there are some radial cracks emanating from the hole, and the number of cracks varies with the standoffs markedly. When the standoff is 0.5 CD, six fragments are formed and the largest fragment with two large cracks and one small crack (the top middle picture in Fig.3). When the standoff is 1.0 CD, two fragments are formed. One fragment with two cracks, and the other with two large cracks and some small cracks (Fig.3(1.0 CD)). When the standoff is 1.5 CD, the steel plate only splits into two fragments and no crack is formed (the bottom left in Fig.3). In addition, the width of crack near the inner surface of hole is larger, due to it is extended from the inner surface of the hole to the outer surface of the plate, and the crack continues to propagate axially

downwards from the upper surface of the plate. It should be noted that the hole diameter from the surface of plate to the bottom of hole is basically of the same widths. The penetration channel and the fracture surface are adhered by some black reactive material detonation products. Moreover, damage effects drop off significantly at 2.0 CD. Even no fragmentation damage pattern but the cracking damage pattern is formed on steel plate when standoff is 2.0 CD. It can be clearly observed that the upper surface of the plate is almost completely covered by black detonation products (the bottom right in Fig.3).

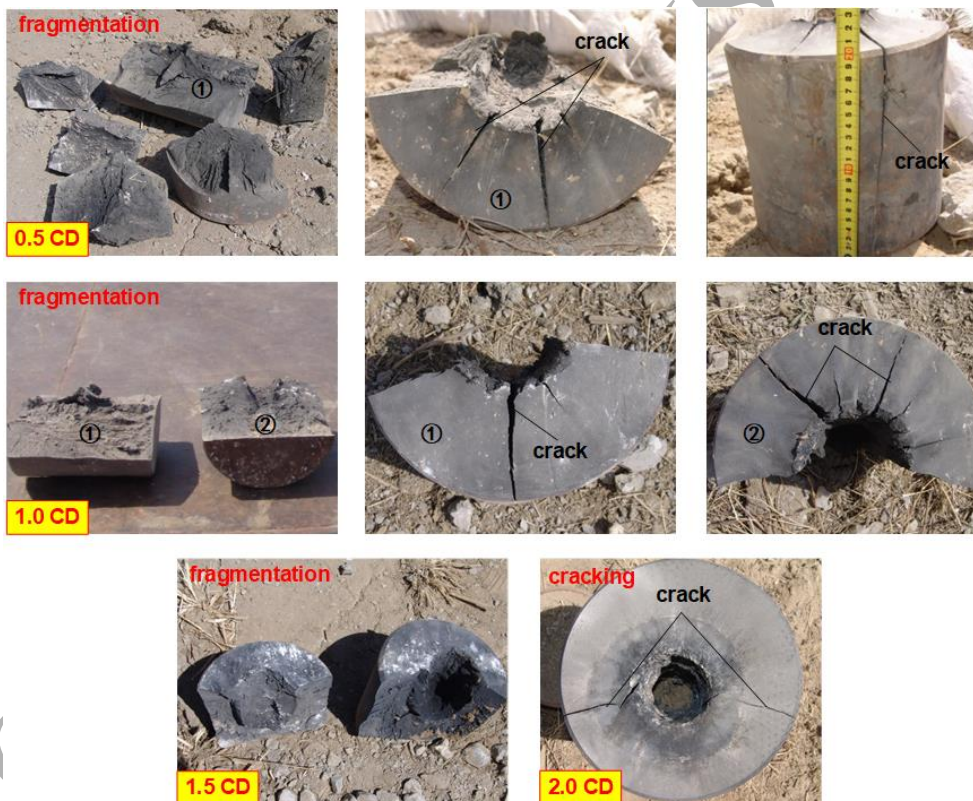


Fig.3 Typical results of penetrating steel plates under different standoffs

3 Penetration model

3.1 Penetration depth

The shock wave generated by main charge detonation not only compresses the

reactive material liner to form a jet, but also activates the reactive materials. As time progresses, the RLSCJ penetrates thick steel plate but won't release its chemical energy until the reactive materials initiate. The period of time from activation to initiation is called initiation delay time of reactive jet, during which assuming RLSCJ penetrates steel plate like metal jet.

Based on the mentioned above assumption, it also assumes that the deflagration of all the reactive materials would not occur immediately until the time arrives at the initiation time of reactive jet, and the chemical energy would be simultaneously released together. Furthermore, ignoring the strength effect of the steel plate, the penetration behavior of RLSCJ impacting thick steel plate can be analyzed based on the virtual origin theory [36]. Fig.4 presents the penetration depth as a function of the penetration time, in which y is the axial distance and y is zero at the bottom of the liner, t is the time and t is zero when the detonation wave reaching the bottom of the charge, t_0 is the time when RLSCJ reaches the upper surface of the steel plate, τ is the initiation delay time of reactive jet, and H is the standoff.

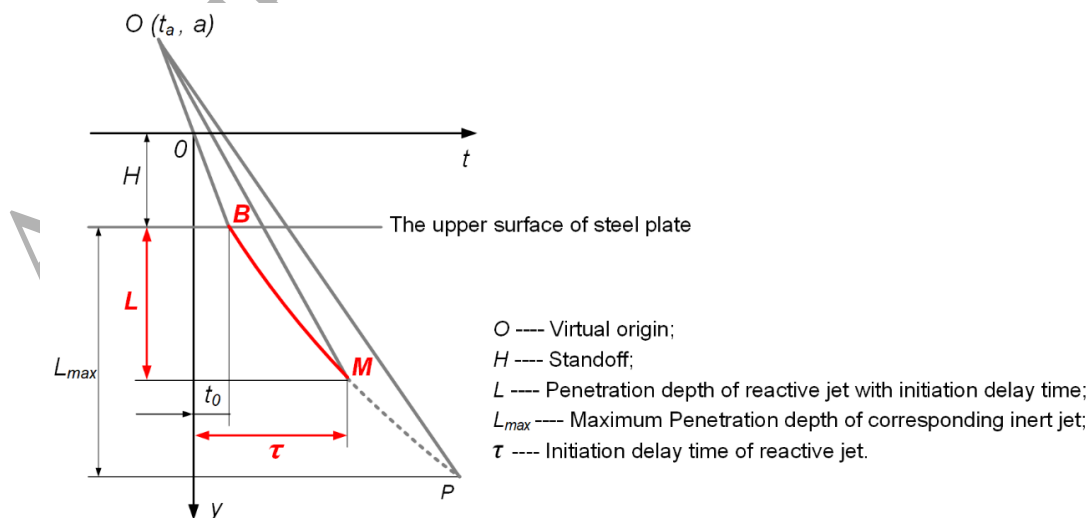


Fig.4 Theoretical model of penetration depth for RLSCJ impacting thick steel plate

Based on the virtual origin theory, the penetration depth is given as

$$L = (H-a) \left[\left(\frac{v_{\text{tip}}}{v_j} \right)^{\sqrt{\rho_j/\rho_t}} - 1 \right] \quad (1)$$

For point M, penetration depth is L , according to the geometric relationship shown in Fig.4

$$(\tau - t_a)v_j = L + H - a \quad (2)$$

Eq. (2) first differential for τ and then integral, the relation can be obtained

$$\tau - t_a = (t_0 - t_a) \left(\frac{v_{\text{tip}}}{v_j} \right)^{1+\sqrt{\rho_j/\rho_t}} \quad (3)$$

Then taking Eq. (3) into Eq. (1), the penetration depth can be rewritten as

$$L = (H-a) \left[\left(\frac{\tau - t_a}{t_0 - t_a} \right)^{\frac{1}{1+\sqrt{\rho_t/\rho_j}}} - 1 \right] \quad (4)$$

Where ρ_t and ρ_j are the density of steel plate and reactive jet, respectively. The coordinates of the virtual origin (t_a , a) can be calculated by numerical simulation, using the least square method.

Combination the Eq. (4) with experimental results, we can obtain four values of initiation delay time due to various errors in the tests process. But for a given shaped charge with reactive material liner, the initiation delay time of reactive jet should be consistent. As such, the initiation delay time of experimental reactive liner material is 126.2 μs , which averaged by fitting the four values of initiation delay time (see Fig.5).

It is apparent that the penetration depth is greatly influenced by initiation delay time of reactive jet and standoff, particularly for the initiation delay time which is the primary determinant of the penetration depth. This relationship can be verified from

the Fig. 5 that the longer initiation delay time of reactive jet (τ), the higher penetration depth (L) could be achieved under given conditions of standoffs and targets. In fact, if the initiation delay time doesn't exist, namely $\tau = 0$, reactive material chemical reaction will occur immediately at the initial moment of the detonation wave impacting reactive liner, and even it can't form a jet so that the penetration depth will be zero. If $\tau < t_0$, the reactive liner can form a reactive jet, but it will have a deflagration before penetrating steel plate, and the penetration depth remains zero. If the initiation delay time is less than the whole penetration time of a corresponding inert jet, the penetration depth will increase as the initiation delay time increase. Nevertheless, if the initiation delay time is sufficiently long, the penetration depth will reach the maximum value (L_{\max}), and the effects of the initiation delay time disappear [29]. Hence, the effects of other factors on penetration depth, such as diameter of liner, cone angle, and wall thickness, are considered only when reactive materials chemical reaction is not occurring significantly during jet formation, as shown in Table 2.

Table 2 shows that, comparing experiment 1 with 2, the penetration depth increases with the decrease of the cone angle, which is consistent with the penetration performance of inert metal jet against steel plate. However, by comparing experiments 2, 3 and 4, the penetration depth drops off significantly with the reduction of the liner wall thickness and the charge diameter, which is not accordance with the similarity principle of metal liner. This is mainly because the absolute wall thickness of reactive liner reduces with the decrease of the charge diameter, the thinner reactive liner will bear a larger explosive detonation pressure and then form a higher velocity jet, by

which will exacerbate and accelerate the chemical reaction of reactive material. As such, the absolute wall thickness has a marked effect on the initiation delay time of reactive jet, which falls with the decrease of the absolute wall thickness, thus resulting in the decline of penetration depth. Combined with the standoff experiments in this paper, the results indicate that the penetration depth and the damaging capability of RLSHJ against thick steel plates are significantly affected by standoff, and the terminal damage effects are better in a region between 0.5 CD and 1.5 CD. However, the analytical model reveals that the influence of initiation delay time on the penetration depth is relatively independent of standoff, but the effect of standoff on penetration depth must be dependent on the formation of reactive jet without chemical reaction. Further investigation of the experiments manifest that when the initiation delay time of reactive jet is relatively short, the excellent terminal damage effect of thick steel plate is achieved with small standoff. Figure 5 also verifies this phenomenon that the optimum standoff of reactive jet is influenced remarkably by initiation delay time, increasing the initiation delay time can appropriately improve the optimum standoff of reactive jet.

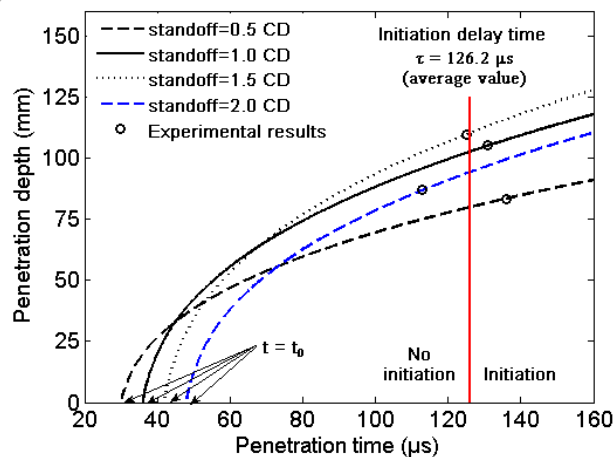


Fig.5 Initiation delay time of reactive jet influencing penetration depth

Table 2 Effects of RLSC parameters on penetration depth [27, 29]

No.	Liner			Standoff (CD)	Penetration depth (CD)
	Diameter (mm)	Cone angle (°)	Thickness (CD)		
1	140	65	0.12	1.0	0.74
2	140	55	0.12	1.0	0.83
3	140	55	0.08	1.0	0.75
4	90	55	0.08	1.0	0.35

As shown in Fig.5, the intersection of the curve with the x-axis indicates the time t_0 , which increases with the increase of standoff, so the time of RLSCJ penetrating steel plate will decrease gradually. In the experiments, as the standoff increases from 0.5 to 1.5 CD, the penetration depth increases, which is mainly caused by the effective stretching of reactive jet and the larger penetration time. However, when the standoff is larger than 1.5 CD, the penetration depth gradually reduces. The first and most important reason is that, due to the same initiation delay time of reactive jet, the penetration time decreases with the increase of standoff, and the reactive jet have a deflagration reaction when the time arrives at the initiation time, which would lead to the early termination of the penetration phase. The second thing must be taken into consideration is that the reactive material liner essentially belongs to the powder metallurgy liner, and the cavitation, necking, or even rupturing occurs more easily at larger standoff, resulting in the decrease of penetration depth. As such, in order to increase the penetration depth of RLSCJ against steel plate, how to improve the

reactive liner material initiation delay time is a very critical factor

3.2 Penetration hole diameter

The formation and penetration of reactive jets under different standoffs were simulated with the two-dimensional axisymmetric model based on the platform of Autodyn code (see Fig.6). The explosive, case, and reactive material liner were meshed by Eulerian algorithm to reduce the great deformation while the steel plate was meshed by Lagrangian algorithm for fracture and fragmentation. The mesh uses a smaller size of 0.5×0.5 mm per cell for the Euler domain of $90 \text{ mm} \times 600 \text{ mm}$, and the mesh size of steel plate is 1.0×1.0 mm. The boundary condition of air (Euler) domain was set as “Flow out (ALL EQUAL)” to eliminate the influence of the boundary effect. Detailed material strength models and EOSs of RLSC each part are shown in Table 3, and main material parameters of the liner, explosive, case, steel plate, and air are listed in Table 4~6.

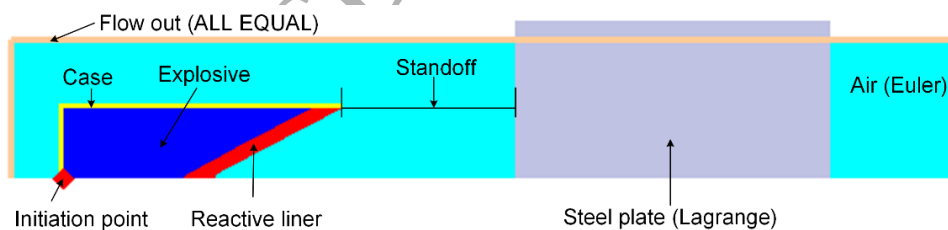


Fig.6 Numerical model (1/2) of RLSC against thick steel plate

Table 3 Material strength models and EOSs of RLSC each part

Part	Materials	EOS	Strength model	Erosion
Air	Air	Ideal Gas	None	None
Liner	Reactive materials	Shock	Johnson Cook	None
Explosive	8701	JWL	None	None

Case	45# steel	Shock	Johnson Cook	None
Steel plate	45# steel	Shock	Johnson Cook	Geometric Strain 1.5

Table 4 Parameters of the reactive liner and steel plate materials [25, 37]

Materials	ρ (kg/m ³)	G (GPa)	A (MPa)	B (MPa)	n	C	m	T_m (K)	T_{room} (K)
Reactive liner	2.27	0.666	8.044	250.6	1.8	0.4	1	500	294
45# steel	7.83	77	792	510	0.26	0.014	1.03	1793	300

Table 5 Parameters of explosive [37]

Material	ρ (kg/m ³)	D (km/s)	P_{CJ} (GPa)	e (GPa)	A (GPa)	B (GPa)	R_1	R_2	ω	v_0
explosive	1.71	8.315	28.6	8.499	524.23	7.678	4.2	1.1	0.34	1.00

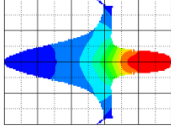
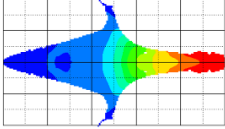
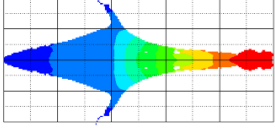
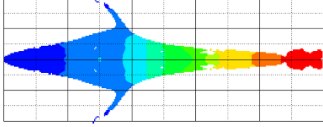
Table 6 Parameters of air [38]

Material	ρ (kg/m ³)	γ	C_p (kJ/kg \cdot K)	C_v (kJ/kg \cdot K)	T (K)	E_0 (kJ/kg \cdot K ⁻¹)
air	1.225	1.4	1.005	0.718	288.2	2.068×10^5

The reactive jet tip velocity (v_{tip}), the tail velocity (v_{tail}), the tip diameter (D_0), the jet length (l_{j0}), and the movement time (see below t_0) when the jet tip reaches the upper surface of steel plate is shown in Table 7. Comparing the velocity distribution of four standoffs, the length of reactive jet increases while the tip velocity and the average jet diameter decrease with the increase of standoff. According to the Held.M radial expansion formula [39], the hole-radius is a function of jet velocity and jet radius. In other words, the tip velocity of reactive jet and jet diameter would decrease

as the standoff increases, resulting in a decrease of hole diameter that occurred at the surface of steel plates.


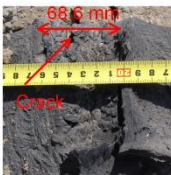
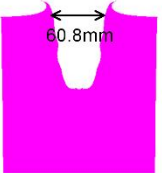
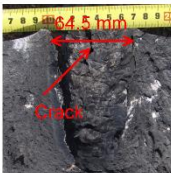
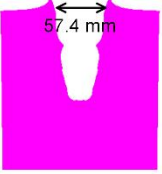
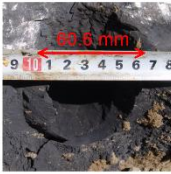


Table 7 Velocity distribution and performance parameters of reactive jets

Standoff	Velocity distribution of jet	v_{tip} (m/s)	v_{tail} (m/s)	D_0 (mm)	l_{j0} (mm)	t_0 (μ s)
0.5 CD		7908	393	18.0	132	29.8
1.0 CD		7759	450	15.8	174	35.7
1.5 CD		7701	538	14.2	215	42.0
2.0 CD		7640	612	12.4	258	48.0

The comparison of simulated and experimental results is illustrated in Table 8. It is obvious that the numerical results of the hole diameter have a good agreement with the experimental data, which demonstrates that the entrance hole diameter will decrease as the standoff increases. However, the simulation results are always smaller than the experiments, and the difference between the two results decreases with the increase of standoff. This may arise for two reasons: (i) The reactive jet has a deflagration in tests, which can further increase the secondary expansion of the hole and even cause fragmentation of the steel plate. (ii) With the standoff increases, the penetration depth and the jet diameter become smaller as a means by which to decrease the effective mass of reactive jet inside the penetration hole. Therefore, with the standoff increases, the secondary expansion cratering effect drops off significantly

by the combined effect of kinetic and chemical energy of reactive materials. Differences between the entrance hole diameter on the steel plate in the experiments and simulations are less than 10% for all the four standoffs, the numerical methods employed in this research could provide effective and accurate solution of the performance parameters of reactive jets.

Table 8 Comparison of experimental and numerical entrance hole diameter

Standoff	Simulation results	Experimental results	Error
0.5 CD			6.85 %
1.0 CD			6.09 %
1.5 CD			5.57 %
2.0 CD			4.58 %

Above all, the hole diameter of RLSCJ penetrating steel plate is generally better than that of traditional metal jet. Mainly for the following three reasons, one is that the larger jet diameter is formed by the larger wall thickness of reactive liner. Secondly, the hardness of reactive material is smaller than that of the metal jet and the deformation in the radial direction is larger, which causing the hole diameter is larger. Finally, the reactive jet has a deflagration when the time arrives at the initiation time,

resulting in the re-expansion cratering effect.

4 Penetration-induced fragmentation behavior

4.1 Effective mass of reactive jet

Based on the velocity distribution of reactive jet before impacting steel plate in Table 7, the jet velocity gradient is very great, which lead to the propagation of reactive jet during the penetration process. We can assume that the reactive jet is a cone penetrator with a linear velocity gradient along its length, described in Fig.7. This assumption domain is suitable for idealized penetration description of reactive jets solved in virtual coordinate frame [40]. Based on the virtual theory, some assumptions of the cone penetrator are made as follows. Firstly, the reactive jet is considered to be divided into infinitesimal elements with the number of n , and the jet is continuous not breaking during penetration. Secondly, each jet element is prolonged, but its volume, density and velocity of each element keep invariable in the penetration process. Thirdly, the velocity gradient is ignored within each jet element. Moreover, with the reactive cone penetrator impacting the steel plate, the velocity of the jet element is not affected by the high pressure, high temperature and high strain rate generated when the previous element penetrates steel plate. As seen the Fig.7, the family of lines start from point O (the virtual origin), and the slope of each line stands for the velocity of the corresponding jet element.

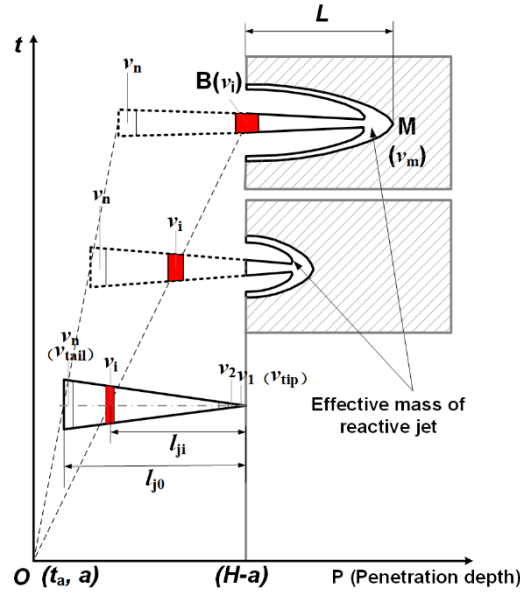


Fig.7 Analytical model for effective mass of reactive jet

Suppose that the reactive cone penetrator does not lose its mass during the penetration process and after the penetrator entering the penetration hole, it will flow along the inner wall of the hole instead of the outside. When the time reaches the reactive jet initiation point, only the reactive materials that occurs deflagration inside the hole can contribute to the secondary structural damage effects while materials outside cannot. This part of reactive materials inside the penetration hole would release huge amounts of chemical energy, which would further enlarge the hole and even lead to the cracking or fragmentation of the thick steel plates. As such, we use the mass of reactive materials inside the hole at the moment of initiation time to represent the effective mass of reactive jet, in solid black line of Fig.7. The effective mass of this portion is marked as m_e , and the mass of outside reactive materials is m_{res} .

For the reactive cone penetrator before impacting the steel plate, the volume of each element can be written as

$$dV = \pi \omega_0^2 l^2 dl \quad (5)$$

Where w_0 is the slope of jet generatrix in the jet coordinate system.

Thus, the effective mass of reactive jet m_e and the initial mass of jet m are obtained as

$$m_e = \rho_j \int_0^{l_{ji}} \pi \omega_0^2 l^2 dl \quad (6)$$

$$m = \rho_j \int_0^{l_{j0}} \pi \omega_0^2 l^2 dl \quad (7)$$

Based on equations (6) and (7),

$$\frac{m_e}{m} = \frac{\rho_j \int_0^{l_{ji}} \pi \omega_0^2 l^2 dl}{\rho_j \int_0^{l_{j0}} \pi \omega_0^2 l^2 dl} = \frac{\int_0^{l_{ji}} l^2 dl}{\int_0^{l_{j0}} l^2 dl} = \left(\frac{l_{ji}}{l_{j0}} \right)^3 \quad (8)$$

As the mentioned above assumptions, the reactive cone penetrator is continuous and the velocity along the length is linear. The relationship l_{ji} / l_{j0} can be replaced by velocity parameters

$$\frac{l_{ji}}{l_{j0}} = \frac{v_{tip} - v_i}{v_{tip} - v_{tail}} = \frac{1 - v_i / v_{tip}}{1 - v_{tail} / v_{tip}} \quad (9)$$

According to the geometric relationship shown in Fig.7, Eq. (10) and (11) can be obtained

$$v_m = \frac{L + H - a}{\tau - t_a} \quad (10)$$

$$v_i = \frac{L + H - a}{\tau - t_a} \quad (11)$$

Then, for the point M, based on the penetration depth Eq. (1), the relation can be written as

$$\frac{v_{tip}}{v_m} = \left(\frac{L}{H - a} + 1 \right)^{\sqrt{\rho_c / \rho_j}} \quad (12)$$

Based on Eq. (10), (11) and (12), the relation can also be written as

$$\frac{v_i}{v_{\text{tip}}} = \left(\frac{L}{H-a} + 1 \right)^{-(1+\sqrt{\rho_i/\rho_j})} \quad (13)$$

Taking Eq. (9) and (13) into (8), the relation between the effective mass of reactive jet and penetration depth can be written

$$\frac{m_e}{m} = \left(\frac{1}{1-v_{\text{tail}}/v_{\text{tip}}} \left(1 - \left(\frac{L}{H-a} + 1 \right)^{-(1+\sqrt{\rho_i/\rho_j})} \right) \right)^3 \quad (14)$$

Where the tip and rear velocity of reactive jet is v_{tip} and v_{tail} , respectively. The value of v_{tip} and v_{tail} can be obtained by numerical simulation.

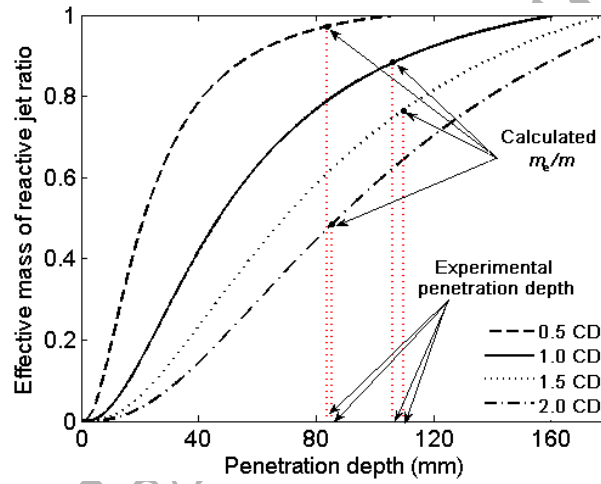


Fig.8 Effective mass of reactive jet as a function of penetration depth

Fig.8 presents the effective mass of reactive jet as a function of penetration depth under different standoffs based on Eq. (14). It shows that the effective mass of reactive jet decreases with the increase of the standoff. The main reason is that when standoff is smaller, the jet is not stretched enough, forming a short and thick cone penetrator, which leads to a higher mass per unit length inside the penetration hole. It is also important to note that the penetration time decreases with the increase of standoff when the initiation delay time of reactive jet is a constant value, resulting in the effective mass of reactive jet inside the penetration hole decreasing.

4.2 Crack generation and propagation

As a result of the initiation delay time of reactive jet, the penetration process of RLSHJ against steel plate consists of two parts: penetration like metal jet and the release of chemical energy contained in reactive materials. Due to the instantaneously great deflagration pressure and the high penetration velocity of reactive jet, it can assume that the penetration hole is a sealed space. To simply analyze, it also assumes that the hole diameter is a constant value from the surface of plate to the bottom of hole based on the experimental results, as shown in Fig.3. As such, based on the failure theory of shell under internal explosion loads [41], the fragmentation process of steel plate involves four phases: elastic-plastic swelling, dynamic crack generation, crack propagation, and fragmentation of the thick steel plates.

Reactive jet has a deflagration reaction when the time after activation reaches the initiation delay time, causing an intensive dynamic stress zone in the penetration hole. At the same time, the detonation-like blast wave will form a compressional stress wave, which would lead to plastic flow in the inner wall of the hole and cause shear failure under the high deflagration pressure. Therefore, the cracks first generate on the inner wall of the hole (see in Fig.9(1) at points A and B). Subsequent unloading waves occur immediately on both sides of the cracks, and the criterion of cracks propagation is that new cracks will not generate in the unloading zone. As such, new cracks may generate randomly at points C, D and E (see in Fig.9(2)). In a word, the same thing will repeatedly happen in the zone which unloading waves do not propagate, and then after unloading waves sweep all zone of the steel plate, cracks will not generate on the

steel plate. The fragmentation process is finished when the steel plate is completely unloaded in two directions, as shown in Fig.9(4).

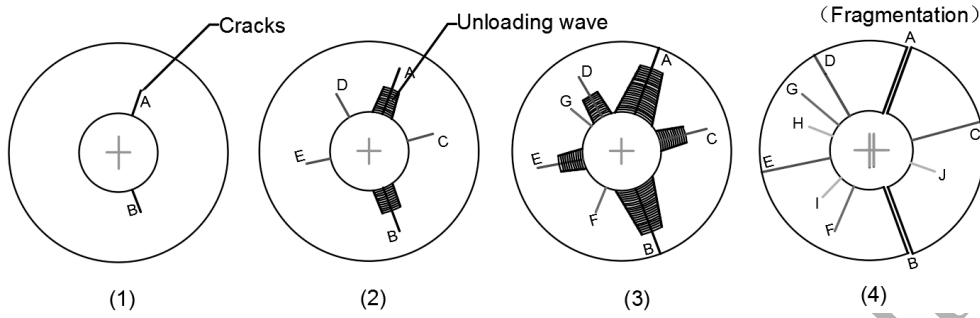


Fig.9. Description of cracks generation and propagation in thick steel plate

4.3 Fragment or crack numbers

Based on Newton's second law, if the width of unloading zone is x , equation of fragmentation behavior of steel plate can be described [41]

$$\sigma_b S = \frac{1}{2g} \rho_t S x \frac{d}{dt} \left(\frac{dx}{dt} \right) \quad (15)$$

Where σ_b is the ultimate strength of the steel plate [MPa], S is the vertical section's area of unloading zone [cm^2], t is the time of unloading wave propagating from 0 to x [s], dx/dt is the tangential deformation velocity of arc length x , which has relation $dx/dt = xv_0/r$, and r is the maximum radius of penetration hole [cm].

Integrate Eq. (15) from 0 to t and 0 to x of time and unloading zone length, respectively. When the thick steel plate generates crack, it assumes that v_0 and r remain unchanged, so the width of unloading zone can be presented as followed

$$x = \frac{2r}{v_0} \sqrt{\frac{\sigma_b g}{\rho_t}} \sqrt{\varepsilon - \varepsilon_k} \quad (16)$$

In which, x is also the fragment size of steel plate, ε is the strain of steel plate after crack generates, ε_k is the critical strain of steel plate. If $S = K\varepsilon$, usually, $\sqrt{\Delta S} =$

$\sqrt{S - S_k} = 1 \sim 2$, we take $\sqrt{\Delta S} = 1.5$, then the average width of the fragment x_0 can be obtained

$$x_0 = 1.5x = \frac{3r}{v_0} \sqrt{\frac{\sigma_b g}{\rho_t K}} \quad (17)$$

As mentioned above the two assumptions, the reactive jet has an instantaneous deflagration and the thickness of shell is a constant value. Therefore, the fragments of the steel plate after detonation have the same initial velocity v_0 . According to these assumptions, we can use the Gurney's equation [42] to calculate the initial velocity of the fragments. It assumes that chemical energy of the effective mass of reactive jet converts to kinetic energy of the fragments and the detonation products 100% during deflagration process, that is

$$m_e \cdot Q_v = \frac{m_t v_0^2}{2} + \frac{m_e v_0^2}{4} \quad (18)$$

In which, Q_v is the energy of reactive materials per unit mass (73.5 wt% PTFE-26.5 wt% Al is just 14151 Jg^{-1}) [29], m_t is the effective mass of cylinder shell [g]. Then the initial velocity can be written

$$v_0 = 2\sqrt{Q_v} / \sqrt{\frac{2m_t}{m_e} + 1} \quad (19)$$

Taking Eq. (19) into Eq. (17), and $\sigma_b = 82 \text{ (kg/mm}^2\text{)}$, $K = 67$ for 45# steel, as a result

$$x_0 = \frac{3r}{2\sqrt{Q_v}} \sqrt{\frac{\sigma_b g}{\rho_t K} \left(\frac{2m_t}{m_e} + 1 \right)} \quad (20)$$

According to the geometric relationship of penetration hole, we can obtain

$$m_t = \frac{1}{4} \pi L \rho_t (D^2 - D_1^2) \quad (21)$$

Where D is the diameter of steel plate, D_1 is the hole diameter and its values are obtained from test results, L is the theoretical penetration depth.

In hence, the number of fragments is expressed as

$$n = \frac{\pi D_1}{x_0} = \frac{4\pi\sqrt{Q_v\rho_t K}}{3\sqrt{\sigma_b g\left(\frac{2m_t}{m_e} + 1\right)}} \quad (22)$$

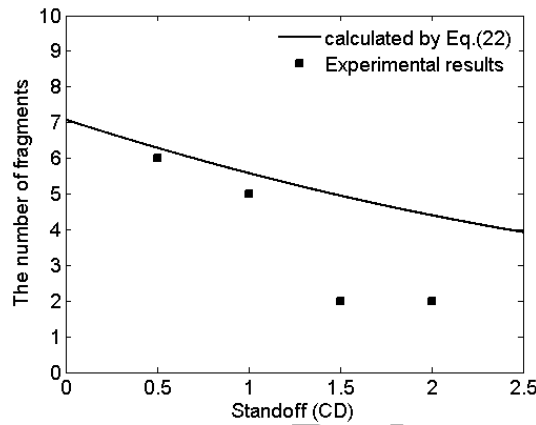


Fig.10 Comparison of model calculations and experiments

In particular, the number of fragments obtained from the test results refers to fragment or large crack numbers, in which the larger cracks seem to be the cracks throughout the upper surface of the thick steel plates. Under the smaller standoffs, especially being within a region between 0.5 CD and 1.0 CD for the shaped charge with reactive liner, the prediction results basically fit well with the experiments, as shown in Fig.10. From the Eq. (22), the number of fragments in the thick steel plates are proportional to the effective mass of reactive jet. When the standoff is 0.5 ,1.0 and 1.5 CD, due to the more effective mass of reactive jet, the pressure produced by the deflagration of reactive materials is much greater than the yield limit of the steel plate, which would cause the steel plates split into several fragments or form many large cracks, as shown in Fig.3. Moreover, when standoff is over 2.0 CD, the effective mass

of reactive jet inside the penetration hole is too little to produce enough pressure to fracture the plate, only generating two cracks.

However, by comparison, the number of fragments calculated by theoretical analysis are almost always bigger than experimental results. Especially under a higher standoff, such deviation becomes larger. On the one hand, the theoretical analysis is not take into account deformation energy of shell, detonation product internal energy, and absorption of media around shell. As such, the initial velocity of theoretical analysis arrives at an optimum limit velocity, resulting in a relative smaller average size of fragments, and then leading to a bigger number of fragments. On the other hand, as the standoff increases, the effective mass of reactive jet inside the penetration hole decreases, which leads to the deflagration pressure and the intensive dynamic loading effect decreases gradually. This tends to approximatively quasi-static loads result in the deviation of analytical results becoming larger gradually.

It should be noted, however, that this analytical model has its own limitations to some extent. One limitation is that the effective mass of reactive jet may be overestimated because of these assumptions that there is no mass loss when RLSCJ penetrates thick steel plate and the whole reactive materials not produce chemical reaction during the jet formation and penetration process. Hence, the number of steel plate fragments calculated based on the effective mass of reactive jet may be overestimated, especially the deviation will be greater when the wall thickness of reactive liner is thicker. This is mainly because the fragmentation effect of thick steel plate depends on the pressure inside the penetration hole, which is not only influenced

by the effective mass of reactive jet but also significantly affected by the energy release rate of reactive materials. Actually, the energy release of reactive jet is linear with time, rather than simultaneous deflagration in the hypothesis, which also may overestimate the number of fragments.

5 Conclusions

The penetration behavior of RLSCJ impacting thick steel plates were studied by experiments and theoretical analyses combined. Several conclusions are presented as follows:

(a) Comparing with the traditional metal liner shaped charge jet, the experiments showed that RLSCJ penetrated thick steel plates to produce larger hole diameter but lower penetration depth. Fragmentation effects and much greater effectiveness could be achieved from the RLSCJ under the relative smaller standoff, especially being within a region between $0.5 C_D$ and $1.5 C_D$.

(b) An model analysis on the influence of initiation delay time of reactive jet and standoff on penetration depth showed that, comparing with the standoff effect, the initiation delay time of reactive jet was the primary determinant of the penetration depth, showing a significantly increase with the increase of the initiation delay time.

(c) The fragmentation damage effects of penetrating steel plates strongly depended on the effective mass of reactive jet inside the penetrating hole and its subsequent deflagration pressure. With the increase of the initiation delay time of reactive jet, the effective mass of reactive jet would increase, resulting in deflagration pressure inside the penetration hole increasing, which caused dramatically cracking or even

fragmentation behavior of the thick steel plates.

Acknowledgments

This research is supported by the National Natural Science Foundation of China (No. U1730112).

References

- [1] DE Technologies, Inc. Reactive Fragment Warhead for Enhanced Neutralization of Mortar, Rocket, and Missile Threats. ONR-SRIR 2006: N04-903:1-7 <http://www.detk.com>.
- [2] Nicolich S. Energetic materials to meet warfighter requirements: an overview of selected US army RDECOM-ARDEC energetic materials programs, 42nd Annual Armament Systems: Gun and Missile Systems Conference, Picatinny Arsenal, NJ.
- [3] A. S. Daniels, E. L. Baker, S. E. DeFisher, et al. Bam Bam: Large Scale Unitary Demolition Warheads. 23rd International Symposium on Ballistics, Tarragona, Spain, 16-20 April 2007.
- [4] B. Grove, J. Heiland, I. Walton, Geologic material's response to shaped charge penetration. *Int J Impact Eng.* 2008,35, 1563-1566.
- [5] Vasant S. Joshi, Process for making Polytetrafluoroethylene-Aluminum composite and product made. U.S. Patent 6547999B1, 2003.
- [6] D. B. Nielson, Richard M. Truitt, Nikki Rasmussen. Low Temperature, Extrudable, High Density Reactive Materials. U.S. Patent 6962634B2, 2005.
- [7] R.J. Lee, W. Mock, Jr., et al. Reactive materials studies. Shock compression of condensed matter. 2005. p. 169–174.
- [8] Mock W Jr, Drotar T. Effect of aluminum particle size on the impact initiation of pressed PTFE/Al composite rods. Shock compression of condensed matter. 2007. p. 971–974.

- [9] Zhang XF, Zhang J, Qiao L, et al. Experimental study of the compression properties of Al/W/PTFE granular composites under elevated strain rates. *Mater. Sci. Eng. A* 2013, 581, 48–55.
- [10] J. Cai, V. F. Nesterenko, K. S. Vecchio, et al. The influence of metallic particle size on the mechanical properties of polytetrafluoroethylene-Al-W powder composites. *Appl. Phys. Lett.* 2008, 92, 031903.
- [11] Wang L, Liu JX, Li SK, et al. Investigation on reaction energy, mechanical behavior and impact insensitivity of WPTFE-Al composites with different W percentage, *Materials and Design*. 2016, 92, 397.
- [12] Ge C, Dong YX, and Maimaitituersun W. Microscale simulation on mechanical properties of Al/PTFE composite based on real microstructures. *Materials*. 2016, 9, 590.
- [13] Li Y, Wang ZC, Jiang CL, et al. Experimental study on impact-induced reaction characteristics of PTFE/Ti composites enhanced by W particles. *Materials*. 2017, 10, 175
- [14] E. M. Hunt, S. Malcolm, M. L. Pantoya, et al. Impact ignition of nano and micron composite energetic materials. *Int. J Impact Eng.* 2009, 36, 842–846.
- [15] Ge C, Dong YX, Maimaitituersun W, et al. Experimental study on impact-induced initiation thresholds of Polytetrafluoroethylene/Aluminum composite. *Propellants Explos. Pyrotech.* 2017, 42, 514–522.
- [16] Zhou J, He Y, He Y, et al. Investigation on Impact Initiation Characteristics of Fluoropolymer-matrix Reactive Materials. *Propellants Explos. Pyrotech.* 2017, 42, 603–615.
- [17] Richard G. Ames. Energy release characteristics of impact-initiated energetic materials. *Proceedings of Materials Research Society Symposium*. Boston: Materials Research Society;

- 2006 p. 0896-H03-08.1-10.
- [18] Richard G. Ames. Vented chamber calorimetry for impact initiated energetic materials. 43rd AIAA Aerospace sciences meeting and exhibit. Reno: Nevada; 2005 p. 279.1-13.
- [19] J. Cai, S. M. Walley, R. J. A. Hunt, et al. High-strain, High-strain-rate Flow and Failure in PTFE/Al/W Granular Composites. *Mater. Sci. Eng. A* 2008, 472, 308–315.
- [20] Wang HF, Zheng YF, Yu QB, et al. Impact-induced initiation and energy release behavior of reactive materials. *J. Appl. Phys.* 2011, 110, 074904.
- [21] Fengyue Xu, Baoqun Geng, Xuepeng Zhang, et al. Experimental study on behind-plate overpressure effect by reactive material projectile. *Propellants Explos. Pyrotech.* 2017, 42, 192-197.
- [22] Lu DW, Wang HF, Lei MA, et al. Enhanced initiation behavior of reactive material projectiles impacting covered explosives. *Propellants Explos. Pyrotech.* 2017, 42, 1117-1123.
- [23] Xu FY, Zheng YF, Yu QB, et al. Experimental study on penetration behavior of reactive material projectile impacting aluminum plate. *Int. J Impact Eng.* 2016, 95, 125-132.
- [24] Xu FY, Yu QB, Zheng YF, et al. Damage effects of double-spaced aluminum plates by reactive material projectile impact. *Int. J Impact Eng.* 2017, 104, 13-20.
- [25] M. N. Raftenberg, W. Mock, G. C. Kirby, Modeling the Impact Deformation of Rods of a Pressed PTFE/Al Composite Mixture. *Int. J. Impact Eng.* 2008, 35, 1735–1744.
- [26] Wang YZ, Yu QB, Zheng YF, et al. Formation and Penetration of Jets by Shaped Charges with Reactive Material Liners. *Propellants Explos. Pyrotech.* 2016, 41, 618-622.
- [27] Jianguang Xiao, Xuepeng Zhang, Zhangxia Guo, et al. Enhanced Damage Effects of Multi-Layered Concrete Target Produced by Reactive Materials Liner. *Propellants Explos.*

- Pyrotech.. 2018, 43:955-961.
- [28] E. L. Baker, A. S. Daniels, K. W. Ng, et al. *Barnie: a Unitary Demolition Warhead*. 19th International Symposium on Ballistics, Interlaken, Switzerland, 23-27 May 2001.
- [29] Xiao JG, Zhang XP, Wang YZ, et al. *Demolition Mechanism and Behavior of Shaped Charge with Reactive Liner*. *Propellants Explos. Pyrotech.* 2016, 41, 612 – 617.
- [30] S. Nicolich. *Reactive material enhanced lethality EFP*. The 42nd Annual Armament Systems: Gun and Missile Systems Conference and Exhibition, Charlotte, USA, 2007.
- [31] T. Rabczuk, T. Belytschko. *Cracking particles: a simplified meshfree method for arbitrary evolving cracks*. *Int. J. Numer. Meth. Engng.* 2004, 61:2316–2343.
- [32] T. Rabczuk, T. Belytschko. *A three-dimensional large deformation meshfree method for arbitrary evolving cracks*. *Comput. Methods Appl. Mech. Engrg.* 196 (2007) 2777–2799.
- [33] T. Rabczuk, G. Zi, S. Bordas, et al. *A simple and robust three-dimensional cracking-particle method without enrichment*. *Comput. Methods Appl. Mech. Engrg.* 199 (2010) 2437–2455.
- [34] Huilong Ren, Xiaoying Zhuang, Yongchang Cai, et al. *Dual-horizon peridynamics*. *Int. J. Numer. Meth. Engng* 2016,108:1451–1476.
- [35] Huilong Ren, Xiaoying Zhuang, Timon Rabczuk. *Dual-horizon peridynamics A stable solution to varying horizons*. *Comput. Methods Appl. Mech. Engrg.* 318 (2017) 762–782.
- [36] Dipersio R, Simon J. *The penetration-standoff relation for optimized shaped charge jets*. BRL Memorandum Report No. 1542, 1964.
- [37] Liu JF, Long Y, Ji C, et al. *The influence of liner material on the dynamic response of the finite steel target subjected to high velocity impact by explosively formed projectile*. *Int. J Impact Eng.* 2017, 109, 264-275.

- [38] Ding LL, Tang WH, Ran XW. Simulation study on jet formability and damage characteristics of a low-density material liner. *Materials*, 2018, 11, 72.
- [39] Held M. Verification of the equation for radial hole growth by shaped charge jet penetration. *Int. J Impact Eng.* 1995, 17(1-3): 387-398.
- [40] D.E. Lambert. Re-visiting 1-D hypervelocity penetration. *Int. J Impact Eng.* 2008, 35:1631-1635.
- [41] The Eighth Department Writing Group of Beijing Institute of Technology. *Explosion and its Effects*. National Defence Industry Press, Beijing, 1979.
- [42] Gurney G W. *The initial velocities of fragments from bombs, shells and grenades [R]*. Aberdeen, Maryland, US: Ballistics Research Laboratories, 1943.